Progress In Electromagnetics Research C, Vol. 89, 149–159, 2019

Near Infrared Supercontinuum Generation in Silica Based Photonic Crystal Fiber

Feroza Begum* **and Pg Emeroylariffion Abas**

Abstract—This research explores a silica based highly nonlinear photonic crystal fiber of near infrared window; solid silica core photonic crystal fiber is suitable for propagating light towards the near-infrared wavelength region. Full vector finite difference method is used for numerical simulation, by solving the generalized nonlinear Schrödinger equation with the split-step Fourier method to show that the design exhibits high nonlinear coefficient, near zero ultra-flattened dispersion, low dispersion slope and very low confinement losses. It is demonstrated that it is possible to generate high power wide supercontinuum spectrum using 2.5 ps input pulses at 1.06 µm, 1.30 µm and 1.55 µm center wavelengths. It is observed that supercontinuum spectrum is broadened from 960 nm to 1890 nm by considering center wavelengths of 1.06 µm, 1.31 µm, and 1.55 µm into silica based index guiding highly nonlinear photonic crystal fiber. Furthermore, immensely short fiber length of 1 m at center wavelengths of 1.06 µm, 1.31 µm and 1.55 µm is possible using the proposed highly nonlinear photonic crystal fiber. The generated high power wide supercontinuum spectrum is applicable as a laser light source in near infrared band.

1. INTRODUCTION

Optical fiber has numerous advantages over other communication mediums. Generally, it is capable of offering high bandwidth with no electrical interference and is relatively easier to install, due to its flexibility. With its core surrounded by a special layer known as cladding, light is able to propagate through the core of the fiber with minimal loss in performance, making it suitable to be used in optical communication, medical imaging and numerous other applications.

Photonic crystal fiber (PCF) is a special type of optical fiber that is gaining popularity and interest in the telecommunication, medical and numerous other industries as well as the research communities. Unlike conventional optical fiber, periodicity in the cladding region of PCF is not crucial, hence, allowing flexibility in its design to suit different applications. Indeed, various designs have been proposed, with varying diameters of air holes in the cladding region, that are able to achieve efficient confinement of guiding light onto the high-index core region of PCF as well as ultra-flattened chromatic dispersion in the broad wavelength range [1, 2]. Other remarkable modal properties are wide range of single-mode operations, zero-dispersion at visible or near-infrared wavelengths and tailorable effective modal areas which cannot be achieved via conventional optical fibers [1, 2].

The design of PCFs with high power and high nonlinear coefficient in addition to near zero dispersion is an active research area, with possible applications in optical communication, supercontinuum (SC) applications and for medical imaging [3, 4]. Applications in the near infrared wavelengths at 1.30 µm and 1.55 µm are of interest for optical communications. For medical imaging especially in ophthalmology and dental applications, operating wavelengths at 1.06 µm and 1.30 µm respectively are applicable due to its minimum dispersion, deep penetration and improved sensitivity [5–7].

Received 1 October 2018, Accepted 7 December 2018, Scheduled 3 January 2019
* Corresponding author: Feroza Begum (feroza.begum@ubd.edu.bn).
The authors are with the Faculty of Integrated Technologies, Universiti Brunei Darussalam, Gadong BE 1410, Brunei Darussal.

Various supercontinuum (SC) generated highly nonlinear photonic crystal fibers (HN-PCFs) have been reported in the literature for optical communications and medical applications [8–22], using different materials to produce broadband SC spectrum with varying performances.

In [8], the authors proposed a highly nonlinear dispersion flattened photonic crystal fiber capable of a large nonlinear coefficient, up to $34\,W^{-1}km^{1}$ at 1.55 μm wavelength for SC generation. The designed highly nonlinear flattened dispersion photonic crystal fiber has four to five different air-hole diameters at different air hole rings, making the design very complex to fabricate. A low-coherence light source was developed in [9], based on Indium Arsenide (InAs) quantum dots superluminescent diode (SLD) with controlled emission wavelengths, which were then applied to optical coherence tomography (OCT) imaging. It is shown that the developed SLDs yield low output power of between 2 mW to 15 mW.

Different designs of femtosecond (fs), picosecend and nanosecond pulse laser sources are proposed and consequently, investigated in references [10–25]. In [10], the authors investigate the performance of femtosecond-laser pulses in neodymium-doped yttrium aluminium garnet (Nd:YAG) crystals and report that output power of around 1.3 W at around 1.0 μm center wavelength is achievable from an 2.25 W launched pump power. A neodymium-(Nd) doped glass laser light source based on PCF for SC spectrum generation is demonstrated in [12]. For average incident pump power of 165 mW, the Nd-doped glass laser light source is able to produce SC spectrum with output power averaging 48 mW at the 1.3 μm center wavelength. Broad SC spectrum generation at a central wavelength of 1.07 μm is reported in [11]; propagating through an 100 metres ytterbium (Yb) doped fiber and generated by noise-like pulses. 10 W power is used to pump the laser to produce 800 mW output power. Instead of using standard fibre, ytterbium doped photonic crystal fiber (Yb doped PCF) is used in [13], capable of generating SC spectrum with a 75 mW output power at a central wavelength of 1.064 μm from a 150 mW input signal wave. Reference [14] studies the performance of a CS_2 core photonic crystal fiber for SC application. It is demonstrated that the PCF is able to generate broadband SC spectrum in the IR region at central wavelength of 1.55 μm, with 100 W pump peak power.

Performances of germanium (GeO_2) doped core fiber are studied in [15, 17]. Highest output power of 13.17 W is obtainable in [15] by applying 34 W input pump power at around 1.0 μm wavelength, using a broadband four stage Er-Yb doped fiber to pump the GeO_2 doped core fiber SC source. Experimental and numerical studies on GeO_2 doped core are demonstrated in [17] producing an average power of 1.8 W femtosecond pulse laser source for pumping at 1.55 μm wavelength.

Stoichiometric silicon nitride (Si_3N_4) integrated optical waveguides are used in [16] to generate broad SC spectrum at the 1.56 μm telecommunication wavelength, with a pulse duration of 120 fs. Maximum average output power of 300 mW is successfully generated through the design in [16]. In [18], the authors demonstrate the generation of ultra-broadband SC spectrun with central wavelengths of 1.55 μm and 1.30 μm, using silica PCF with As_2S_3 chalcogenide glass doped core. The SC generations use femtosecond pulse laser source with 3 kW peak power. Using a laser source with a peak power of 4.4 kW, an ultra-broadband SC spectrum may be generated at 1.55 μm wavelength, by using germanium doped core fiber [19]. Similarly, Ge-doped PCF picosecond pulse laser with 10 W input peak power is investigated in [20], to produce broadband SC spectrum at the 1.31 μm center wavelength.

Supercontinuum (SC) generations have also been demonstrated [21–23], with $Ge_{11.5}As_{24}Se_{64.5}$ chalcogenide glass core [21, 22] and highly nonlinear liquid material core [23]. 1 kW and 100 W input peak powers have been used to generate SC spectrum at 1.55 μm centre wavelength in references [21] and [22], respectively. In [23], SC spectrum with the peak power of 2 kW at 1.55 μm centre wavelength has been successfully demonstrated.

Designs for HN-PCF for applications in OCT and telecommunication (i.e., wavelength between 1.0 to 1.7 μm) are presented in [24–26], shown to be capable of producing supercontinuum (SC) spectrum using picosecond pulses. In [24], maximum launched input peak powers of 50.0 W, 14.0 W and 45.0 W at center wavelengths of 1.06 μm, 1.31 μm, and 1.55 μm, respectively, are demonstrated whilst incident pulse input powers of 43.0 W, 8.0 W and 40.0 W, at center wavelength of 1.06 μm, 1.31 μm and 1.55 μm, respectively, are demonstrated in [25]. Supercontinuum spectra at centre wavelengths of 1.3 μm and 1.65 μm are generated in [26] with input peak power of 1.38 kW. Designs in [24–26] utilise silicon dioxide as the core of their HN-PCFs.

As can be noted from the experimental and numerical results obtained in [9–26], relatively low-power SC spectrum is generated from some of the designs with varying material types. The exhibited

low-power SC spectrum may not be sufficient for some SC applications. Most of the designs, with the exception of the designs in [24–26], also utilise doped core fiber structures, which are relatively difficult to fabricate for mass production of the materials. Furthermore, it needs to be noted that femtosecond pulse laser-based SC sources has a relatively high implementation cost as compared to other pulse laser sources.

In this respect, it is important to produce fiber that is able to generate ultra-broadband SC spectrum with high power, preferably utilising picosecond pulse laser source. This is because picosecond pulse laser has high single pulse energy, high peak power, high nonlinear effects especially self-phase modulation (SPM) and stimulated Raman scattering (SRS). Furthermore, output supercontinuum source has orderly pulsed trains with good time coherence and wide flat spectrum. Consideration must also be given to the structure of the fiber to ensure that the design is easily fabricatable.

In this paper, picosecond pulse based HN-PCFs shall be proposed that is relatively simple to fabricate whilst exhibiting favourable performance characteristics. It shall be shown that the simple HN-PCF model has high nonlinear coefficients of more than 105 $[\text{Wkm}]^{-1}$ at 1.06 µm, 72 $[\text{Wkm}]^{-1}$ at 1.31 µm and 52 $[\text{Wkm}]^{-1}$ at 1.55 µm, exhibits a very low confinement loss of less than 10^{-7} dB/km from 1.0 µm to 1.6 µm wavelength range and ultra-flattened chromatic dispersion in the targeted wavelength range. Full vector finite difference method (FDM) shall be used to calculate different properties of the proposed HN-PCFs. High input powers of 2.5 kW, 4.0 kW and 6.0 kW are obtainable at 1.06 µm, 1.30 µm and 1.55 µm center wavelengths, respectively for generating broad SC spectrum. Furthermore, extremely short fiber length of 1 m may be obtained at center wavelengths of 1.06 µm, 1.31 µm and 1.55 µm. The proposed HN-PCF simultaneously exhibits high nonlinear coefficients, extremely low confinement loss, ultra-flattened chromatic dispersion, high incident power and very short length fiber with potential for the optical communications and medical applications.

2. PROPOSED HIGHLY-NONLINEAR PHOTONIC CRYSTAL FIBRE (HN-PCF)

Figure 1 shows the geometry of the proposed PCFs structure, with regular silica-based core surrounded by seven (7) rings of air holes of three (3) different diameters. The first (i.e., innermost) and fourth rings of air holes have diameters d_1 and d_2, respectively, whilst the rest of the rings (i.e., the second, third, fifth until seventh rings of air hole) have diameters d. Distance between centers of neighboring air holes (i.e., its pitch) is kept Λ apart.

For the design of silica-based HN-PCF, it is required that the PCF is able to control dispersion at the near infrared window with sufficient field confinement. It is known that the size of the air-

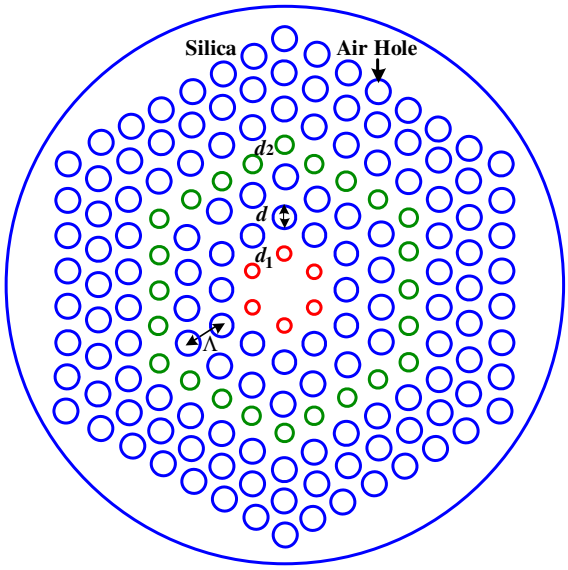

Figure 1. Structure of the proposed HN-PCF with air hole arrangement.

holes near the PCF core affects the dispersion characteristics [27, 28], and hence, the dimensions of the first and fourth rings of the proposed silica based HN-PCFs are scaled downed to shape its dispersion characteristics. The dimensions of the other rings are, however, kept sufficiently large to allow for better field confinement. This is in contrast to conventional PCFs structure with identical diameters for all the air holes.

To demonstrate the resultant characteristics of the proposed design, chromatic dispersion, confinement loss and effective area shall be analyzed at the near infrared window. The main advantage of this HN-PCF is that it produces high nonlinearity, providing ultra-broadband SC spectrum without using any doping in its core.

3. NUMERICAL METHOD

Finite difference method (FDM) [29–34] with anisotropic perfectly matched layers (PML) is used in this study to investigate the performance of the proposed HN-PCF. Modal effective refractive index n_{eff} may be obtained by solving an eigenvalue problem drawn from the Maxwell's equations using FDM. Subsequently, chromatic dispersion parameter $D(\lambda)$, chromatic dispersion slope $D_{\mathrm{s}}(\lambda)$, confinement loss parameter L_c, effective area A_{eff} [29–32] and nonlinear coefficient parameter γ [33] may be calculated. It is noted that material dispersion given by the Sellmeier equation is included in the chromatic dispersion parameter calculation. Nonlinear Schrödinger equation (NLSE) [33], used for the numerical calculation of supercontinuum (SC) spectrum, is solved using the Split-step Fourier method.

$$D(\lambda) = -\frac{\lambda}{\mathrm{c}}\frac{\partial^2 \mathrm{Re}\left[n_{eff}\right]}{d\lambda^2} \tag{1}$$

$$D_S(\lambda) = \frac{\partial D(\lambda)}{\partial \lambda} \tag{2}$$

$$L_C = 8.686 k_0 \mathrm{Im}\left[n_{eff}\right] \tag{3}$$

$$A_{eff} = \frac{2\pi\left(\int_0^\infty |E_a(r)^2|rdr\right)^2}{\int_0^\infty |E_a(r)|^4 rdr} \tag{4}$$

$$\gamma = \frac{n_2\omega}{cA_{eff}} = \frac{2\pi n_2}{\lambda A_{eff}} \tag{5}$$

where

$D(\lambda)$: Chromatic dispersion parameter [ps/(nm · km)]
$D_s(\lambda)$: Chromatic dispersion slope parameter [ps/(nm^2 · km)]
L_c: Confinement loss parameter [dB/km]
A_{eff}: Effective area parameter [μm^2]
γ: Nonlinear coefficient parameter [W^{-1}km^{-1}]
n_{eff}: Modal effective refractive index, consisting of real and imaginary components
Re[n_{eff}]: Real component of n_{eff}
Im[n_{eff}]: Imaginary component of n_{eff}
λ: Operating wavelength [μm]
c: Velocity of light in a vacuum
d: Diameter of the 4th–8th rings of air hole
$k_0 = \frac{2\pi}{\lambda}$: Wave number in free space
E_a: Electric field
r: Radial distance
n_2: Non-linear refractive index coefficient in the nonlinear part of the refractive index

The following NLSE equation is used for SC spectrum numerical computation [33].

$$\frac{\partial A}{\partial z} + \frac{\alpha}{2}A + \frac{i}{2}\beta_2\frac{\partial^2 A}{\partial T^2} - \frac{1}{6}\beta_3\frac{\partial^3 A}{\partial T^3} = i\gamma\left[|A|^2 A + i\frac{\lambda_c}{2\pi c}\frac{\partial}{\partial T}(|A|^2 A) - T_R A\frac{\partial |A|^2}{\partial T}\right] \quad (6)$$

where

z: Propagation length
A: Optical field complex amplitude
T: Time
α: Fiber absorption coefficient
λ_c: Center wavelength
T_R: Raman gain slope
β_n: Propagation constant of n-th order with $n = 1, 2, 3$.

4. SIMULATION RESULTS AND DISCUSSIONS

Simulation of the proposed HN-PCF in Fig. 1 is performed with the diameters of the first and fourth rings of air holes set at $d_1 = 0.32\,\mu m$ and $d_2 = 0.36\,\mu m$, respectively. The diameters of the remaining air holes are fixed at $d = 0.79\,\mu m$ with air hole spacing, i.e., pitch set at $\Lambda = 0.87\,\mu m$. Chromatic dispersion, chromatic dispersion slope, confinement loss, effective area and nonlinear coefficient parameter are then calculated using Equations (1)–(6) and plotted in Figs. 2–6 below.

4.1. Chromatic Dispersion and Chromatic Dispersion Slope

Figures 2(a) and (b) show the chromatic dispersion and chromatic dispersion slope for different operating wavelengths between 1.0 µm and 1.6 µm. From Fig. 2(a), it can be seen that the proposed HN-PCF exhibits ultra-flattened chromatic dispersion over the observed wavelength of between 1.0 µm to 1.6 µm, with chromatic dispersion values of approximately -2.81, 0.45 and $-0.60\,ps/(nm \cdot km)$ at wavelengths of 1.06, 1.30 and 1.55 µm, respectively. Within the 500 nm flat wavelength band ranging from 1100 nm to 1600 nm, which is part of near infrared and short wavelength infrared bands, dispersion variation of approximately $0.5\,ps/(nm \cdot km)$ is observed. Correspondingly, it is shown in Fig. 2(b) that the proposed HN-PCF exhibits a near zero negative dispersion slope over the observed wavelength. This represents the possibility of efficient supercontinuum generation, as small dispersion slope value is necessary to allow for smaller pulse broadening in the wide bandwidth ranges.

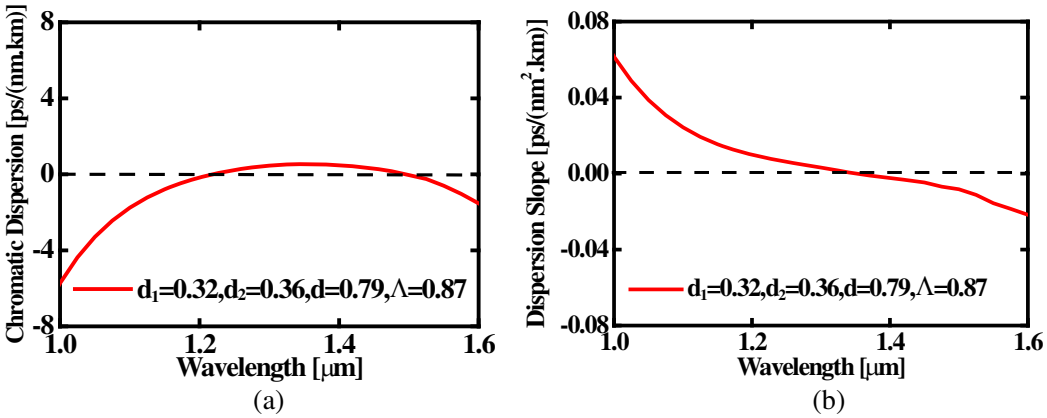

Figure 2. (a) Chromatic dispersion and (b) chromatic dispersion slope values as a function of wavelength.

4.2. Effective Area and Nonlinear Coefficient

Figures 3(a) and (b) demonstrate the effective area and nonlinear coefficient as a function of operating wavelengths of between 1.0 μm and 1.6 μm. Nonlinear coefficient is inversely proportional to the effective area, as shown in Equation (5). As high nonlinear coefficient is necessary for the generation of effective supercontinuum spectrum, in turns it can be said that small effective area is also a necessity. These two requirements are exhibited in the proposed HN-PCF. At the operating wavelengths of 1.06 μm, 1.30 μm and 1.55 μm, the effective areas of the HN-PCF are 1.76 μm^2, 2.06 μm^2 and 2.38 μm^2, respectively, whilst the corresponding nonlinear coefficients of more than 105 $W^{-1}km^{-1}$, 72 $W^{-1}km^{-1}$ and 52 $W^{-1}km^{-1}$, respectively, are observed from the figures.

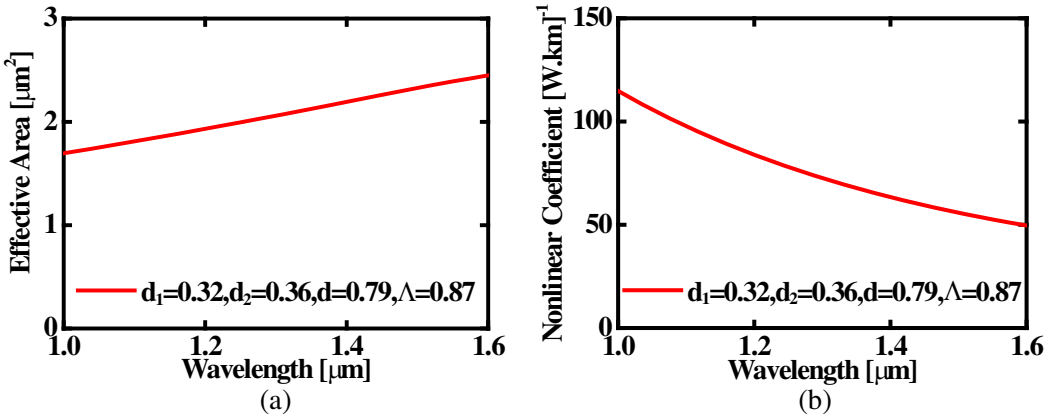

Figure 3. (a) Effective area and (b) nonlinear coefficient values as a function of wavelength.

4.3. Confinement Loss

Confinement loss L_c of the proposed HN-PCF for different operating wavelengths between 1.0 μm and 1.6 μm is illustrated in Fig. 4, with confinement loss less than 10^{-7} dB/km over all observed wavelengths. Reduction in confinement loss may be achieved by either increasing the number of air holes in the cladding region or increasing the size of the air holes. The choice on the large value of d for the proposed HN-PCF is made for this purpose.

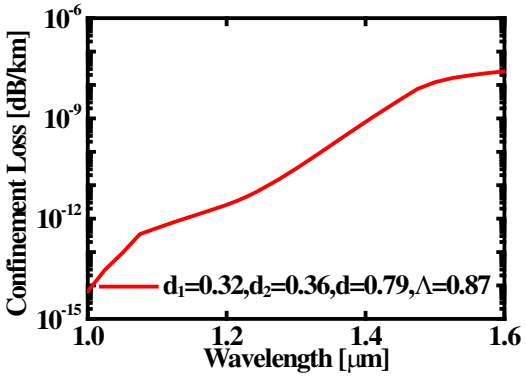

Figure 4. Confinement loss values as a function of wavelength.

4.4. Chromatic Dispersion Comparison

The proposed HN-PCF is also compared with a similar PCF structure to that of the proposed HN-PCF but with only the first ring of air holes having a reduced diameter, referred to as basis PCF.

This comparison is to observe the effect of reducing the diameter of the fourth ring of air holes whilst keeping everything constant, on chormatic dispersion of the PCF. Structure-wise comparisons between the proposed HN-PCF and the basis PCF are given in Table 1.

Table 1. Structural comparison between the proposed HN-PCF and the basis PCF.

Notations	Description	Basis PCF	Proposed HN-PCF
d_1	Diameter of the first ring of air holes	0.32 µm	0.32 µm
d_2	Diameter of the first ring of air holes	0.79 µm	0.36 µm
d	Diameter of all other rings except the 1st and the 4th	0.79 µm	0.79 µm
Λ	Distance between centre of air holes i.e., pitch	0.87 µm	0.87 µm

Chromatic dispersion comparison between the proposed HN-PCF and the basis PCF is given in Fig. 5 over operating wavelength between 1.0 µm and 1.6 µm. It is noted that the blue and red lines in the figure depict the chromatic dispersions of the basis PCF and HN-PCF, respectively. Reducing the diameter of the fourth ring of air holes shifts up the chromatic dispersion line. As such, appropriate pitch and air hole diameter selections are very important to obtain a flat and near zero chromatic dispersion.

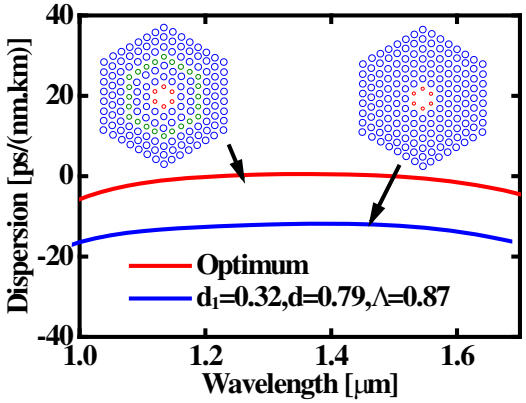

Figure 5. Comparison of chromatic dispersion values as a function of wavelength.

4.5. Supercontinuum Spectrum

Supercontinuum generation in the proposed high power HN-PCF is numerically calculated using Equation (6) above, for centre wavelength λ_c values of 1.06 µm, 1.30 µm and 1.55 µm, and plotted in Figs. 6(a), (b) and (c), respectively. Sech^2 waveform propagation with full width at half maximum (FWHM), T_{FWHM} of 2.5 ps, is considered, with Raman scattering parameter T_R of 3.0 fs through the proposed silica based HN-PCF. Propagation constants around the carrier frequency β_2 and β_3 used in the calculations are given in Table 2 for the three (3) different centre wavelengths considered in this study.

From the figures, it can be seen that the spectrum width increases with increase in centre wavelength. For centre wavelength at 1.06 µm in Fig. 6(a), spectrum range is between 950 nm and 1200 nm, i.e., width of 250 nm. The width increases to 380 nm for centre wavelength of 1.30 µm in Fig. 6(b), with range between 1140 nm and 1520 nm, and further increases to 580 nm for centre wavelength of 1.55 µm in Fig. 6(c), with range between 1300 nm to 1900 nm. Numerical simulation is also performed to obtain the incident pulse input powers P_{in} at different centre wavelengths; incident pulse input powers P_{in} of 2.5 kW, 4.0 kW and 6.0 kW are obtained at centre wavelength values of 1.06 µm, 1.30 µm and 1.55 µm, respectively. Acquired fiber length L_F is 1 m for all the center wavelengths.

Table 2. Propagation constants around the carrier frequency for different centre wavelengths under consideration.

Propagation constants with different order		β_2 (ps^2/km)	β_3 (ps^2/km)
Centre Wavelength λ_c	1.06 µm	1.013	0.022
	1.30 µm	−1.524	0.023
	1.55 µm	2.166	0.019

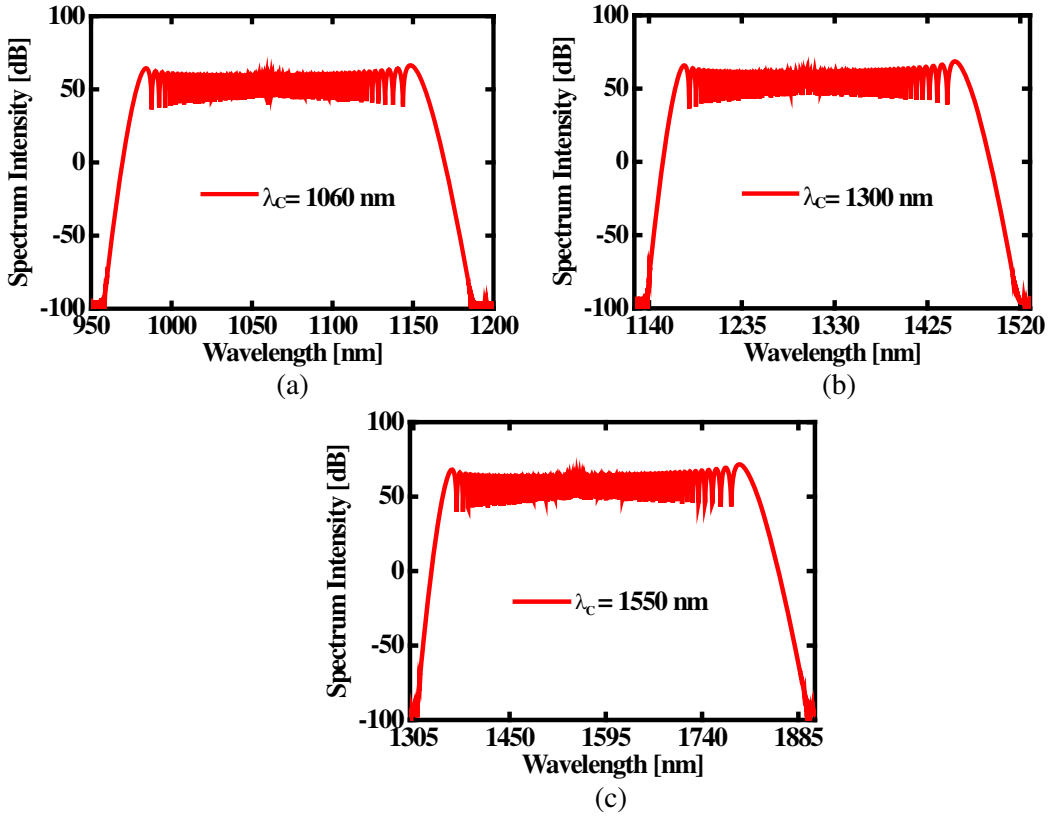

Figure 6. Numerically simulated optical spectrum as a function of wavelength for (a) $\lambda_c = 1.06\,\mu$m, $P_{\text{in}} = 2.5\,$kW; (b) $\lambda_c = 1.30\,\mu$m, $P_{\text{in}} = 4.0\,$kW; and (c) $\lambda_c = 1.55\,\mu$m, $P_{\text{in}} = 6\,$kW.

4.6. Power Comparison

Comparison is also made between the proposed HN-PCF, particularly at the centre wavelength values of 1.0 µm, 1.30 µm and 1.55 µm, and other fibers available in the literature [8–26] in terms of coherent power. This comparison is depicted in Table 3, showing fabricated fiber materials, center wavelength and coherent powers of the different optical fibers considered. It should be highlighted that all the fibers considered are doped fibers with the exception of the fibers in [8, 24–26] and the proposed HN-PCF in this paper.

It can be clearly seen from the table that the proposed HN-PCF achieves higher power values than other fibers [8–26]. Furthermore, the proposed HN-PCF is un-doped and hence, is relatively easier to fabricate than doped fiber.

Table 3. Comparison between the properties of proposed HN-PCF with other designed fiber.

Reference	Material	λ_c [μm]	Coherent power
[8]	Silica PCF	1.55	6.0 W
[9]	InAs quantum dot SLD	1.19	15.0 mW
[10]	Nd-doped YAG crystal	1.063	2.25 W
[11]	Yb doped fiber	1.070	10.0 W
[12]	Nd doped glass	1.3	165.0 mW
[13]	Yb doped PCF	1.064	150.0 mW
[14]	CS_2 core PCF	1.55	100.0 W
[15]	GeO_2 doped core	1.55	34.0 W
[16]	Si_3N_4 optical waveguide	1.56	300 mW
[17]	GeO_2 doped core	1.56	1.8 W
[18]	As_2S_3 chalcogenide core	1.30, 1.55	3.0 kW, 3.0 kW
[19]	Germania core	1.55	4.4 kW
[20]	Ge doped core PCF	1.31	10.0 W
[21]	Chalcogenide PCF	1.55	1.0 kW
[22]	Chalcogenide rib waveguide	1.55	100 W
[23]	Liquid-core PCF	1.55	2 kW
[24]	Silica PCF	1.06, 1.31, 1.55	50.0 W, 14.0 W, 45.0 W
[25]	Silica PCF	1.06, 1.31, 1.55	43.0 W, 8.0 W, 40.0 W
[26]	Silica PCF	1.30	1.38 kW
Proposed HN-PCFs	Silica PCF	1.06, 1.31, 1.55	2.5 kW, 4.0 kW, 6.0 kW

5. CONCLUSION

In this paper, a highly nonlinear PCF with air holes in the fiber cladding region, with reduced diameters for the first and fourth rings of air holes, has been proposed and successfully analysed using FDM method. The proposed fiber exhibits near zero ultra-flattened chromatic dispersion coefficient, small chromatic dispersion slope and extremely low confinement loss in the 1.0 μm to 1.6 μm wavelength range, making it suitable for optical transmission systems. Moreover, it has a high nonlinear coefficient, allowing usage for laser light source within the infrared bands. A very short fiber length may also be achieved from the proposed HN-PCF.

As such, the proposed HN-PCF may be suitable for different applications such as chromatic dispersion controller, in nonlinear optical systems, and for efficient supercontinuum generation in the infrared region. It is also a promising candidate for optical transmission and as a light source in medical imaging because of the generated supercontinuum spectrum.

REFERENCES

1. Knight, J. C., "Photonic crystal fibres," *Nature*, Vol. 424, 847–851, 2003.
2. Knight, J. C., T. A. Birks, P. St. J. Russell, and D. M. Atkin, "All-silica single-mode optical fiber with photonic crystal cladding," *Optics Letters*, Vol. 21, No. 19, 1547–1549, 1996.
3. Begum, F., Y. Namihira, S. M. A. Razzak, S. Kaijage, N. H. Hai, T. Kinjo, K. Miyagi, and N. Zou, "Design and analysis of novel highly nonlinear hexagonal photonic crystal fibers with ultra-flattened chromatic dispersion," *Optics Communications*, Vol. 282, No. 7, 1416–1421, 2009.

4. Begum, F., Y. Namihira, T. Kinjo, and S. Kaijage, "Supercontinuum generation in photonic crystal fibers at 1.06 μm, 1.31 μm and 1.55 μm wavelengths," *Electronics Letters*, Vol. 46, No. 22, 1518–1520, 2010.
5. Colston, Jr., B. W., U. S. Sathyam, L. B. DaSilva, M. J. Everett, P. Stroeve, and L. L. Otis, "Dental OCT," *Opt. Express*, Vol. 3, No. 6, 230–238, 1998.
6. Namihira, Y., J. Liu, T. Koga, F. Begum, M. A. Hossain, N. Zou, S. F. Kaijage, Y. Hirako, H. Higa, and M. A. Islam, "Design of highly nonlinear octagonal photonic crystal fiber with near-zero flattened dispersion in 1.31 μm Waveband," *Optical Review*, Vol. 18, No. 6, 436–440, 2011.
7. Izatt, J. A. and M. A. Choma, *Optical Coherence Tomography*, 47–72, Professor Dr. Wolfgang Drexler, Professor Dr. James G. Fujimoto, ed., Springer Publisher, 2008.
8. Saitoh, K., M. Koshiba, T. Hasegawa, and E. Sasaoka, "Highly nonlinear dispersion-flattened photonic crystal fibers for supercontinuum generation in a telecommunication window," *Opt. Express*, Vol. 12, No. 10, 843–852, 2004.
9. Shibata, H., N. Ozaki, T. Yasuda, S. Ohkouchi, N. Ikeda, H. Ohsato, E. Watanabe, Y. Sugimoto, K. Furuki, K. Miyaji, and R. A. Hogg, "Imaging of spectral-domain optical coherence tomography using a superluminescent diode based on InAs quantum dots emitting broadband spectrum with Gaussian-like shape," *Japanese Jour. of Appl. Phys.*, Vol. 54, 04DG07-1–04DG07-5, 2015.
10. Calmano, T., J. Siebenmorgen, O. Hellmig, K. Petermann, and G. Huber, "Nd:YAG waveguide laser with 1.3 W output power, fabricated by direct femtosecond laser writing," *Appl. Phys. B*, Vol. 100, 131–135, 2010.
11. Zaytsev, A., C.-H. Lin, Y.-J. You, C.-C. Chung, C.-L. Wang, and C.-L. Pan, "Supercontinuum generation by noise-like pulses transmitted through normally dispersive standard single-mode fibers," *Opt. Express*, Vol. 21, No. 13, 16056–16062, 2013.
12. Aguirre, A. D., N. Nishizawa, J. G. Fujimoto, W. Seitz, M. Lederer, and D. Kopf, "Continuum generation in a novel photonic crystal fiber for ultrahigh resolution optical coherence tomography at 800 nm and 1300 nm," *Opt. Express*, Vol. 14, No. 3, 1145–1160, 2006.
13. Louot, C., B. M. Shalaby, E. Capitaine, S. Hilaire, P. Leproux, D. Pagnoux, and V. Couderc, "Supercontinuum Generation in an Ytterbium-Doped Photonic Crystal Fiber for CARS Spectroscopy," *IEEE Photonics Technol. Letters*, Vol. 28, No. 19, 2011–2014, 2016.
14. Raj, G. J., R. V. J. Raja, N. Nagarajan, and G. Ramanathan, "Tunable broadband spectrum under the influence of temperature in IR region using CS_2 core photonic crystal fiber," *Journal of Lightwave Technol.*, Vol. 34, No. 15, 3503–3509, 2016.
15. Jain, D., R. Sidharthan, P. M. Moselund, S. Yoo, D. Ho, and O. Bang, "Record power, ultra-broadband supercontinuum source based on highly GeO_2 doped silica fiber," *Opt. Express*, Vol. 24, No. 23, 26667–26677, 2016.
16. Porcel, M. A. G., F. Schepers, J. P. Epping, T. Hellwig, M. Hoekman, R. G. Heideman, P. J. M. V. D. Slot, C. J. Lee, R. Schmidt, R. Bratschitsch, C. Fallnich, and K.-J. Boller, Two-octave spanning supercontinuum generation in stoichiometric silicon nitride waveguides pumped at telecom wavelengths," *Opt. Express*, Vol. 25, No. 2, 1542–1554, 2017.
17. Tarnowski, K., T. Martynkien, P. Mergo, K. Poturaj, G. Sobon, and W. Urbanczyk, "Coherent supercontinuum generation up to 2.2 μm in an all-normal dispersion microstructured silica fiber," *Opt. Express*, Vol. 24, No. 26, 30523–30536, 2016.
18. Ali, R. A. H., M. F. O. Hameed, and S. S. A. Obayya, "Ultrabroadband supercontinumm generation through photonic crystal fiber with As_2S_3 chalcogenide core," *J. Lightwave Techn.*, Vol. 34, No. 23, 5423–5430, 2016.
19. Yang, L., B. Zhange, K. Yin, J. Yao, G. Liu, and J. Hou, "0.6–3.2 μm supercontinuum generation in a step-index germanium-core fiber using a 4.4 kW peak-power pump laser," *Opt. Express*, Vol. 24, No. 12, 12600–12606, 2016.
20. Namihira, Y., M. A. Hossain, T. Koga, M. A. Islam, S. M. A. Razzak, S. F. Kaijage, Y. Hirako, and H. Higa, "Design of highly nonlinear dispersion flattened hexagonal photonic crystal fibers for dental optical coherence tomography applications," *Opt. Review*, Vol. 19, No. 2, 78–81, 2012.

21. Karim, M. R., H. Ahmad, and B. M. A. Rahman, "All-normal dispersion chalcogenide PCF for ultraflat mid-infrared supercontinuum generation," *IEEE Photonics Technology Letters*, Vol. 29, No. 21, 1792–1795, 2017.
22. Ahmad, H., M. R. Karim, and B. M. A. Rahman, "Modeling of dispersion engineered chalcogenide rib waveguide for ultraflat mid-infrared supercontinuum generation in all-normal dispersion regime," *Applied Physics B*, Vol. 124, No. 3, Article 47, 2018.
23. Guo, Z., J. Yuan, C. Yu, X. Sang, K. Wang, B. Yan, L. Li, S. Kang, and X. Kang, "Highly coherent supercontinuum generation in the normal dispersion liquid-core photonic crystal fiber," *Progress In Electromagnetics Research M*, Vol. 48, 67–76, 2016.
24. Begum, F., Y. Namihira, T. Kinjo, and S. Kaijage, "Broadband supercontinuum spectrum generated highly nonlinear photonic crystal fiber applicable to medical and optical communication systems," *Japanese Journal of Applied Physics*, Vol. 50, 092502–092507, 2011.
25. Begum, F. and Y. Namihira, "Design of supercontinuum generating photonic crystal fiber at 1.06, 1.31 and 1.55 µm wavelengths for medical imaging and optical transmission systems," *Natural Science*, Vol. 3, No. 5, 401–407, 2011.
26. Mohamed, L. F., C. Lynda, and H. Issam, "Supercontinuum generation in silica photonic crystal fiber at 1.3 µm and 1.65 µm wavelengths for optical coherence tomography," *Optik*, Vol. 152, No. 1, 106–115, 2018.
27. Poletti, F., V. Finazzi, T. M. Monro, N. G. R. Broderick, V. Tse, and D. J. Richardson, "Inverse design and fabrication tolerances of ultra-flattened dispersion holey fibers," *Opt. Express*, Vol. 13, No. 10, 3728–3736, 2005.
28. Shen, L.-P., W.-P. Huang, and S.-S. Jian, "Design of photonic crystal fibers for dispersion-related applications," *J. Lightw. Technol.*, Vol. 21, No. 7, 1644–1651, 2003.
29. Zhu, Z. and T. Brown, "Full-vectorial finite-difference analysis of microstructured optical fibers," *Opt. Express*, 10, No. 17, 853–864, 2002.
30. Guo, S., F. Wu, S. Albin, H. Tai, and R. Rogowski, "Loss and dispersion analysis of microstructured fibers by finite-difference method," *Opt. Express*, Vol. 12, No. 15, 3341–3352, 2004.
31. Begum, F., Y. Namihira, S. M. A. Razzak, and N. Zou, "Novel Square photonic crystal fibers with ultra-flattened chromatic dispersion and low confinement losses," *IEICE Transaction on Electronics*, Vol. E90-C, No. 3, 607–612, 2007.
32. Bjarklev, A., J. Broeng, and A. S. Bjarklev, *Photonic Crystal Fibers*, Kluwer Academic Publishers, 2003.
33. *Supercontinuum Generation in Optical Fibers*, J. M. Dudley and J. R. Taylor (eds.), Cambridge University Press, 2010,
34. Sellmier, W., "Zur Erklärung der abnormen Farbenfolge im Spektrum einiger Substanzen," *Annalen der Physik*, Vol. 219, No. 6, 272–282, 1871.